How to cite: *Angew. Chem. Int. Ed.* **2023**, *62*, e202305737
doi.org/10.1002/anie.202305737

Graphene Nanostructures | Hot Paper

Bottom-up Solution Synthesis of Graphene Nanoribbons with Precisely Engineered Nanopores

Wenhui Niu, Yubin Fu, Gianluca Serra, Kun Liu, Jörn Droste, Yeonju Lee, Zhitian Ling, Fugui Xu, José D. Cojal González, Andrea Lucotti, Jürgen P. Rabe, Michael Ryan Hansen, Wojciech Pisula, Paul W. M. Blom, Carlos-Andres Palma, Matteo Tommasini, Yiyong Mai, Ji Ma,* and Xinliang Feng**

Abstract: The incorporation of nanopores into graphene nanostructures has been demonstrated as an efficient tool in tuning their band gaps and electronic structures. However, precisely embedding the uniform nanopores into graphene nanoribbons (GNRs) at the atomic level remains underdeveloped especially for in-solution synthesis due to the lack of efficient synthetic strategies. Herein we report the first case of solution-synthesized porous GNR (**pGNR**) with a fully conjugated backbone via the efficient Scholl reaction of tailor-made polyphenylene precursor (**P1**) bearing pre-installed hexagonal nanopores. The resultant **pGNR** features periodic subnanometer pores with a uniform diameter of 0.6 nm and an adjacent-pores-distance of 1.7 nm. To solidify our design strategy, two porous model compounds (**1a**, **1b**) containing the same pore size as the shortcuts of **pGNR**, are successfully synthesized. The chemical structure and photophysical properties of **pGNR** are investigated by various spectroscopic analyses. Notably, the embedded periodic nanopores largely reduce the π-conjugation degree and alleviate the inter-ribbon π–π interactions, compared to the nonporous GNRs with similar widths, affording **pGNR** with a notably enlarged band gap and enhanced liquid-phase processability.

Introduction

Nanoscale pores in graphene nanostructures play a critical role in modifying their geometry, electronic, and mechanical properties depending on the shape, size, and density of the nanopores.[1] Especially, graphene nanoribbons (GNRs) with various regularly structured nanopores have attracted growing attention in recent years due to their unique topology, magnetic, and thermoelectric transport properties, providing potential applications in ion transport, gas sensing, thermoelectric devices, etc.[2] Taking advantage of on-surface chemistry, porous GNRs with well-defined nanopores have been recently achieved from rationally designed monomers on metal surfaces under ultra-high vacuum

[*] Dr. W. Niu, Dr. Y. Fu, Dr. J. Ma, Prof. Dr. X. Feng
Max Planck Institute of Microstructure Physics
Weinberg 2, 06120 Halle (Germany)
E-mail: ji.ma@tu-dresden.de
xinliang.feng@tu-dresden.de

Dr. W. Niu, Dr. Y. Fu, K. Liu, Dr. J. Ma, Prof. Dr. X. Feng
Center for Advancing Electronics Dresden (cfaed) & Faculty of Chemistry and Food Chemistry, Technische Universität Dresden
Mommsenstrasse 4, 01062 Dresden (Germany)

Dr. W. Niu, Dr. F. Xu, Prof. Dr. Y. Mai
School of Chemistry and Chemical Engineering, Frontiers Science Center for Transformative Molecules, Shanghai Key Laboratory of Electrical Insulation and Thermal Ageing, Shanghai Jiao Tong University
Shanghai 200240 (P. R. China)
E-mail: mai@sjtu.edu.cn

G. Serra, Dr. A. Lucotti, Prof. Dr. M. Tommasini
Dipartimento di Chimica, Materiali e Ingegneria Chimica "G. Natta", Politecnico di Milano
Piazza Leonardo da Vinci 32, 20133 Milano (Italy)

J. Droste, Prof. Dr. M. Ryan Hansen
Institute of Physical Chemistry, Westfälische Wilhelms-Universität Münster
Corrensstraße 28/30, 48149 Münster (Germany)

Y. Lee, Dr. J. D. Cojal González, Prof. Dr. J. P. Rabe, Prof. Dr. C.-A. Palma
Department of Physics & IRIS Adlershof—Humboldt-Universität zu Berlin
12489 Berlin (Germany)

Z. Ling, Prof. Dr. W. Pisula, Prof. Dr. P. W. M. Blom
Max Planck Institute for Polymer Research
Ackermannweg 10, 55128 Mainz (Germany)

Prof. Dr. C.-A. Palma
Beijing National Laboratory for Condensed Matter Physics, Institute of Physics, Chinese Academy of Sciences
Beijing 100190 (P. R. China)

J. Droste
Institut für Organische Chemie, Leibniz Universität Hannover
Schneiderberg 1B, 30167 Hannover (Germany)

Prof. Dr. W. Pisula
Department of Molecular Physics, Faculty of Chemistry, Lodz University of Technology
Zeromskiego 116, 90-924 Lodz (Poland)

conditions and then in situ characterized by scanning probe techniques (Figure 1a). For example, N-doped GNRs with periodic planar nanopores on Ag(111) were synthesized using a silver-assisted Ullmann-type polymerization of brominated tetrabenzophenazine.[3] Later on, porous GNRs with nonplanar pores on Au(111) were also independently prepared using 10,21-dibromohexabenzo[*a,c,fg,j,l,op*]tetracene[4a] or 5,8-dibromopicene[4b] as monomer via Ullmann-like coupling and subsequent cyclodehydrogenation. While there has been preliminary progress in on-surface synthesis, the resultant porous GNRs always contain C–C single bonds (highlighted in red, Figure 1a), which inevitably disrupt their intact conjugation. In addition, the aforementioned porous GNRs suffer from the low yield and the substantial challenge of transferring them onto "technical" substrates for further characterizations.

In order to understand more intrinsic properties of porous GNRs and explore their future applications, it is essential to develop wet chemistry methods for producing well-defined porous GNRs with high efficiency, large-scale production, and good liquid-phase processability.[5] In the past years, only a few π-extended polycyclic aromatic hydrocarbons (PAHs or nanographenes) with defined nanopores from the dendritic oligophenylene precursors have been achieved via in-solution synthesis, such as the C108 and C216 featuring a single hexagonal nanopore (Figure 1b).[6] However, the bottom-up solution synthesis of expanded porous GNRs with periodic, well-defined nanopores remains elusive due to the lack of efficient synthetic strategies and appropriate precursor designs. In this work, we demonstrate the first solution-synthesized fully conjugated porous GNR (**pGNR**) using A_2B_2 Suzuki polymerization of bis-boronic ester macrocyclic monomer and another dihalogenated monomer, followed by a cyclodehydrogenation reaction (Figure 1c). The tailor-made macrocyclic monomer with phenanthrene units and pre-installed hexagonal pore is essential to achieve the intact conjugation and precise porous structure of **pGNR**. As a result of this exquisite design, the resultant **pGNR** possesses periodic hexagonal pores with a diameter of 0.6 nm (carbon-to-carbon) and adjacent-pores-distance of 1.7 nm (Figure 1c). The chemical identity of **pGNR** was unambiguously verified by Fourier-transform infrared spectroscopy (FT-IR), Raman and solid-state NMR spectroscopies as well as supported by the successful synthesis of two model compounds with the same hexagonal nanopore (**1a** and **1b**). Density functional theory (DFT) simulation suggests that the nanopores in **pGNR** can effectively modulate its electronic structure and energy levels distribution in comparison to its nonporous counterpart. The resultant **pGNR** exhibits good dispersibility and a well-resolved absorption with a maximum peak at 568 nm in tetrahydrofuran (THF), corresponding to an enlarged optical band gap of ~2.0 eV, compared with the reported solution-synthesized GNRs with similar widths that present the band gaps from 1.1 to 1.88 eV,[7,8] in good line with the calculated tendency. Our study paves the way for solution synthesis of porous GNRs with well-defined pores, tunable band gaps, and liquid-phase processability, enabling their potential integrations in filtering, sensing and thermoelectric devices.

Results and Discussion

Porous model compounds **1a** and **1b**, which can be considered as the short segments of **pGNR**, were synthesized to evaluate our synthetic design strategy, as depicted in Scheme 1. First, compound 1-(4-bromophenyl)dodecan-1-one (**2**) was prepared in 58% yield via Friedel–Crafts

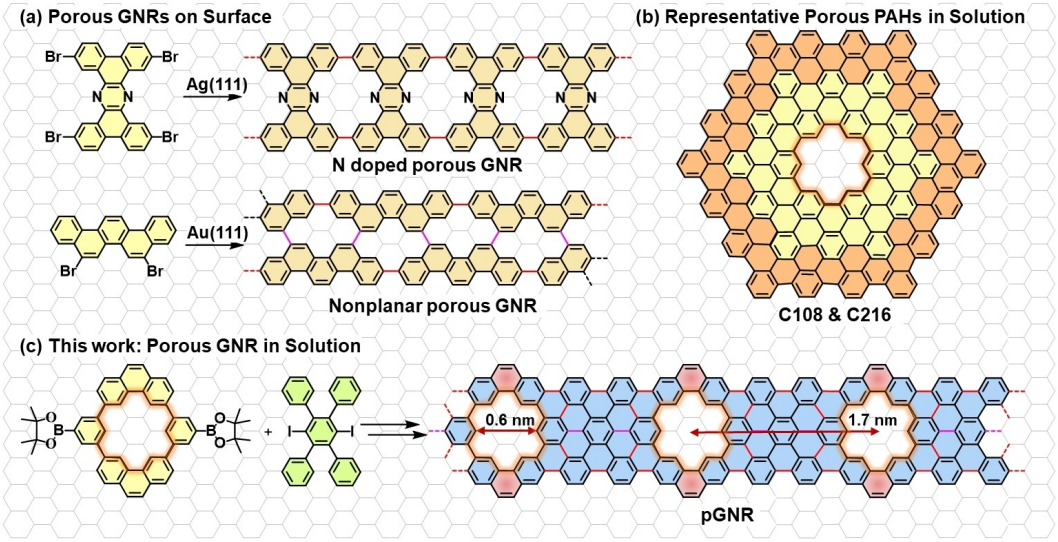

Figure 1. (a) On-surface synthesized two porous GNRs where the single bonds are highlighted in red. (b) Solution-synthesized porous nanographenes C108 (yellow background) and C216 (yellow and orange background). (c) Solution-synthesized porous GNR (**pGNR**) in this work. Alkyl chains are omitted for clarity.

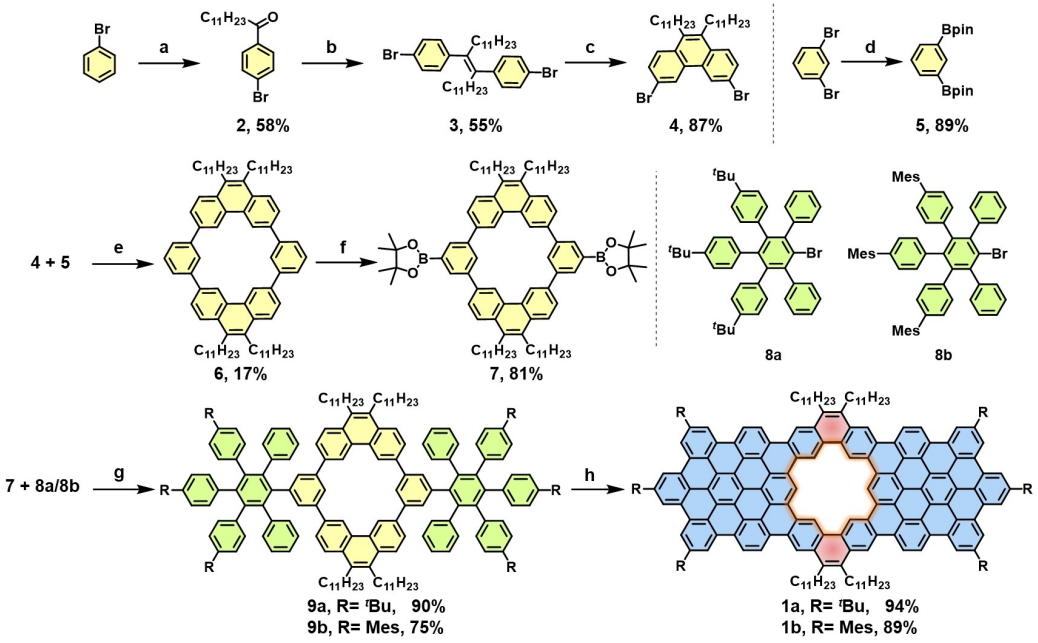

Scheme 1. Schematic illustration of the synthesis of model compounds **1a** and **1b**. (a) Lauroyl chloride, $AlCl_3$, 50 °C, 2 h; (b) $TiCl_4$, Zn, pyridine, THF, reflux, 24 h; (c) I_2, propylene oxide, *hν*, toluene, r.t., overnight; (d) B_2pin_2, $Pd(dppf)Cl_2$, KOAc, DMSO, 80 °C, overnight; (e) $Pd_2(dba)_3$, [(*tert*-Bu)$_3$PH]BF_4, $NaHCO_3$, THF, H_2O, 80 °C, 3 days; (f) B_2pin_2, $[Ir(OMe)cod]_2$, 4,4′-di-*tert*-butyl-2,2′-bipyridine, cyclohexane, 80 °C, overnight; (g) $Pd(PPh_3)_4$, K_2CO_3, dioxane, H_2O, 80 °C, 20 h, **9a** or **9b**; (h) $FeCl_3$, CH_3NO_2, CH_2Cl_2, 0 °C, 1 h for **1a** or 15 min for **1b**.

acylation of the commercially available bromobenzene. Then, **2** was converted into 4,4′-(tetracos-12-ene-12,13-diyl)bis(4-bromobenzene) (**3**) by McMurry reaction in 55 % yield. With the 300 nm light irradiation of **3**, 3,6-dibromo-9,10-diundecylphenanthrene (**4**) was obtained in a good yield of 87 %. 1,3-bis(4,4,5,5-tetramethyl-1,3,2-dioxaborolan-2-yl)benzene (**5**) was prepared by Miyaura borylation from 1,3-dibromobenzene in 89 % yield. After that, the Suzuki coupling between **4** and **5** at dilute concentration gave macrocyclic 1,3(3,6)-diphenanthrena-2,4(1,3)-dibenzenacyclobutaphane (**6**) with a yield of 17 %. The subsequent Ir-catalyzed direct C–H borylation gave the key building block 2,2′-(1^9,1^{10},3^9,3^{10}-tetraundecyl-1,3(3,6)-diphenanthrena-2,4(1,3)-dibenzenacyclobutaphane-2^5,4^5-diyl)bis(4,4,5,5-tetramethyl-1,3,2-dioxaborolane) (**7**) in 81 % yield. Meanwhile, the penta-substituted bromobenzene **8a** and **8b** with different substituents were synthesized following the reported strategy[9] (see details in SI), respectively. Afterward, the Suzuki coupling between **7** and **8a** or **8b** provided the precursor **9a** or **9b** with pre-installed hexagonal nanopore in a yield of 90 % or 75 %, respectively. To our delight, the Scholl reaction of **9a** and **9b** gave the target porous nanographenes **1a** and **1b** with excellent isolated yields (**1a**, 94 %; **1b**, 89 %) by using iron chloride ($FeCl_3$, 2.5 equiv/H) as the Lewis acid and oxidant.

We first confirmed the successful formation of model compounds **1a** and **1b** using MALDI-TOF MS analysis, where the observed isotopic distribution patterns matched well with the calculated spectra (Figure 2a). However, due to the severe π–π interaction of the model compounds, their characterization by solution NMR spectroscopy was not possible (Figure S1). Then we conducted FT-IR (Figure 2b), FT-Raman (Figure 2c) measurements and compared the experimental results with DFT-calculated spectra to confirm the structural identity of model compound **1a**. The agreement between the observed and computed IR spectra of **1a** is excellent (Figure 2b). In particular, the simulation associates the intense band measured at 863 cm^{-1} to collective out-of-plane C–H bending normal modes localized both on the outer edge and in the pore of the molecule; therefore, such a band is recognized as a vibrational marker of the pore. Remarkably, this band (863 cm^{-1}) corresponds to the same marker observed at 857 cm^{-1} in the IR spectrum of a nanographene (C216) with the same kind of cavity.[6a] The peak observed at 809 cm^{-1} is assigned to the DUO (doubly adjacent CHs) mode, localized at the edge of the nanographene. The experimental and simulated Raman spectra of **1a** also display a good agreement (Figure 2c). The expected D and G bands are respectively measured at 1340 and 1611 cm^{-1} and correspond to peaks computed at 1331 and 1619 cm^{-1}. In particular, the D peak is associated with the characteristic ring-breathing modes coupled with in-plane C–H bending and CH_2 wagging modes. The G peak appears as the convolution of several features displaying C–C stretching modes either along the longitudinal or the diagonal direction, coupled in most cases with in-plane C–H bending modes. Thus, the observed good correspondence between the vibrational spectra simulated by DFT and the experiments supports the successful synthesis of model compounds (Table S1, S2). Low-temperature scanning tunneling microscopy (LT-STM) confirms the porous structure of **1a** (Figure 2d, unmasked regions), following annealing of the drop-casted solutions of **1a** on Au(111)/mica substrates under ultrahigh vacuum (see Supporting Information).

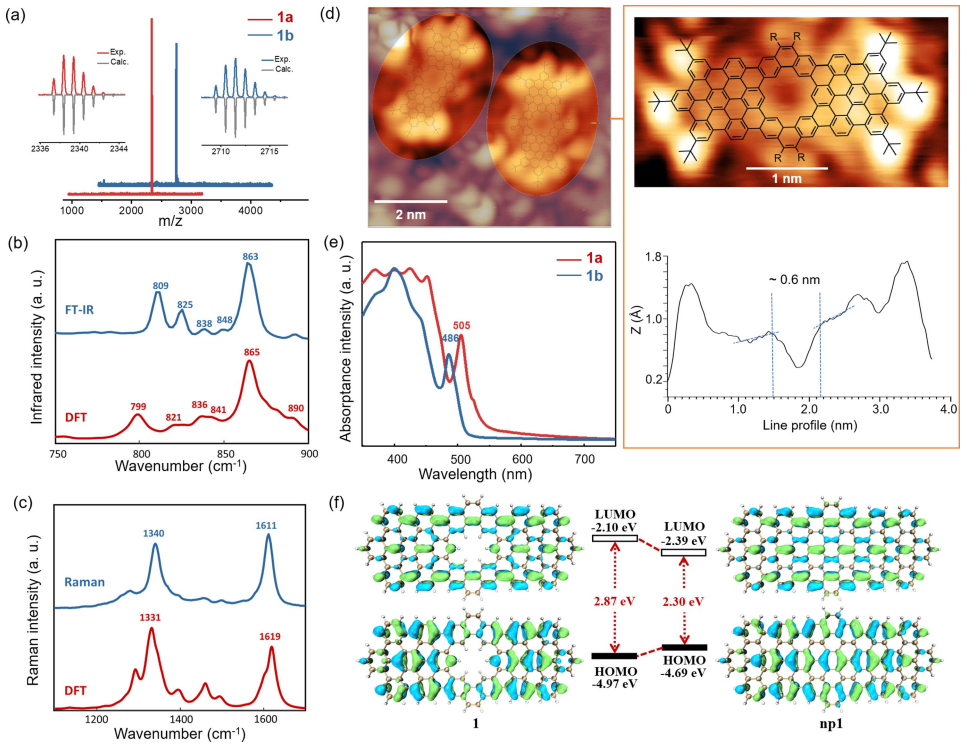

Figure 2. (a) High-resolution MALDI-TOF mass spectra of **1a** and **1b**. Experimental and simulated FT-IR (b) and Raman (c) spectra of **1a** normalized to unity. Some peaks are labelled with their corresponding peak position in units of cm^{-1}. (d) LT-STM observation of **1a** on Au(111)/mica at 5.1 K following heat treatment > 200 °C of the solution-deposited material (see Supporting Information). Tunneling current $I_t = 100$ pA and $U_s = 1$ V. The background has been masked to highlight individual molecules. Detail of a single molecule of **1a** showing triplet of bright units assigned to the *t*-Bu groups. The STM topographic profile size identifies the pore diameter amounting to ~0.6 nm as compared to the DFT model with a pore diameter of 0.59 nm (carbon-to-carbon) or 0.37 (hydrogen-to-hydrogen). The molecular model is superposed according to the scale derived from DFT. (e) UV/Vis absorption spectra of **1a** and **1b** in CH_2Cl_2. (f) Molecular orbitals and their energy diagrams calculated by TD-DFT at the B3LYP/6-31G(d) level of **1** and **np1**, respectively.[13]

Annealing over 200 °C helps desorb most contaminants from the substrate. In the process, the alkyl chains of **1a** appear to detach from the molecular backbone, as previously observed with cove-GNRs deposited on BN/Cu(111).[10] The resultant molecules are therefore encountered in a disordered adsorbate matrix that is tentatively assigned to solvent and detached alkyl chains. The LT-STM detail in Figure 2d depicts three bright protrusions at the sides of the molecule, wherein *t*-Bu groups are identified. The nanopore diameter is ~0.6 nm, which is consistent with the calculated diameter of the pore (0.6 nm, carbon-to-carbon), in accordance to the previous STM imaging of hexagonal nanopores.[3,11] To gain information about the self-assembly of the porous model compounds, the organization of **1b** in thin film is investigated by grazing-incidence wide-angle X-ray scattering (GIWAXS) (Figure S2). The film of **1b** is prepared by drop casting from a THF solution at 2 mg/ml and slow solvent evaporation to ensure a homogeneous film formation and high molecular order. Atomic force microscopy (AFM) image in Figure S3 shows a highly smooth surface morphology of **1b**. The profile of the GIWAXS pattern of **1b** reveals two major scattering peaks that are assigned to the interlayer spacing of 29.2 Å and the stacking distance of 3.9 Å (Figure S2). The observed interlayer distance corresponds well with the molecular spacing in the STM image for **1a** in Figure 2d and intercolumnar distances found for extended discotic nanographenes.[12]

The UV/Vis absorption spectra of model compounds **1a** and **1b** in anhydrous CH_2Cl_2 solutions were presented in Figure 2e. The spectrum of **1a** with *t*-Bu substituents exhibited a maximum absorption peak (λ_{max}) at 505 nm and an absorption onset was observed at 534 nm, corresponding to an optical energy gap of 2.32 eV. Notably, compound **1b** functionalized bulky mesityl groups presented improved solubility due to the reduced π–π aggregation. Thus, the absorption peak of compound **1b** blue-shifted from 505 to 486 nm compared to **1a**, featuring an energy gap of 2.42 eV estimated from an absorption onset at 512 nm. To gain insight into the perturbation of the electronic structure from nanopores, DFT calculations at the B3LYP/6-31G(d) level were performed for pristine porous model compound **1** and its nonporous counterpart (**np1**) (Figure 2f),[11] in which the substitutions of both compounds are removed to simplify the calculations. For both **1** and **np1**, the highest occupied molecular orbital (HOMO) and lowest unoccupied molecular orbital (LUMO) are delocalized over the entire conjugated backbone, revealing that the presence of nanopore in the model compounds does not break the molecular conjugation skeleton. In addition, DFT calculated HOMO and LUMO energy levels as well as the energy gaps are

labeled in Figure 2f. Notably, compared with the molecular orbitals of **np1**, the porous compound **1** presents a lower HOMO and a higher LUMO value, leading to an enlarged energy gap (2.87 for **1** *vs* 2.30 eV for **np1**). The results demonstrate that the embedded nanopores can fine-tune the electronic structures of nanographenes. Moreover, time-dependent (TD)-DFT calculations reveal that the maximum absorption peaks of **1** (calculated value of 415 nm) and **np1** (calculated value of 526 nm) can be both assigned to the mixed contributions of HOMO-1→LUMO and HOMO→LUMO+1 transitions (Table S7).

Encouraged by the successful synthesis of model compounds, we then carried out the synthesis of the related **pGNR** in solution, as illustrated in Scheme 2. First, the dihalogen 4,4″-didodecyl-4′,5′-bis(4-dodecylphenyl)-3′,6′-diiodo-1,1′:2′,1″-terphenyl (**10**) was synthesized following the literature.[14] Then, the A_2B_2-type Suzuki polymerization of monomers **7** and **10** was performed to furnish the polyphenylene precursor (**P1**) in 90% yield using $Pd(PPh_3)_4$ as catalyst and K_2CO_3 as base in dioxane and water refluxing for 3 days. The reaction mixture was precipitated in MeOH and the resulting white powder was collected as the crude polymer **P1**. The MALDI-TOF mass spectrum of the resultant powder revealed that the m/z intervals are in good agreement with the exact mass of the repeating unit (AB = 2172 g mol^{-1}) (Figure 3a). Moreover, each peak in the mass spectrum can be assigned to a specific oligomer with a certain number of units A and B (Figure 3a, inset). After that, the large-molecular weight fraction of the polyphenylene precursor **P1** was fractionated with the help of recycling preparative gel permeation chromatography (GPC). The analytical GPC analysis against linear polystyrene standard disclosed that the number-average molecular weight (M_n) of **P1** is around 25 kg mol^{-1} with a narrow dispersity of ~1.32 (Figure S6). Finally, **pGNR** was achieved through the Scholl reaction of **P1** with $FeCl_3$ (7.5 equiv/H) as the Lewis acid and oxidant in CH_2Cl_2 at room temperature for 3 days. The **pGNR** possesses periodic hexagonal pores in the backbone with a (carbon-to-carbon) diameter of 0.6 nm and adjacent-pores-distance of 1.7 nm (Scheme 2a). The estimated average length of **pGNR** is about 20 nm based on the M_n of **P1**. Furthermore, DFT simulation confirms the planar conformation of **pGNR** due to the appropriate strain of the hexagonal nanopores in the ribbon skeleton, in line with the above planar model compounds (Scheme 2b, Figure S7).

The successful synthesis of **pGNR** was first confirmed by FT-IR (Figure 3b) and FT-Raman (Figure 3c) investigations. DFT accounts well for the intense IR band measured at 865 cm^{-1}, which is assigned to out-of-plane C–H bending modes both in the pore and at the edge of the GNR. Moreover, the peak observed at 809 cm^{-1} in the FT-IR spectrum of **1a** is absent in this case, as expected based on the chemical structure of **pGNR** which lacks DUO C–H bonds. The agreement is also good for the observed Raman spectrum of **pGNR** and its computational counterpart. In this case, the broad D peak, measured at 1335 cm^{-1}, is associated with several modes involving ring-breathing modes in different regions of **pGNR** and coupled with in-plane C–H bending modes. The G peak at 1611 cm^{-1} displays two degenerate C–C stretching modes along the diagonal direction, with a minor contribution along the longitudinal direction. The graphical representation of

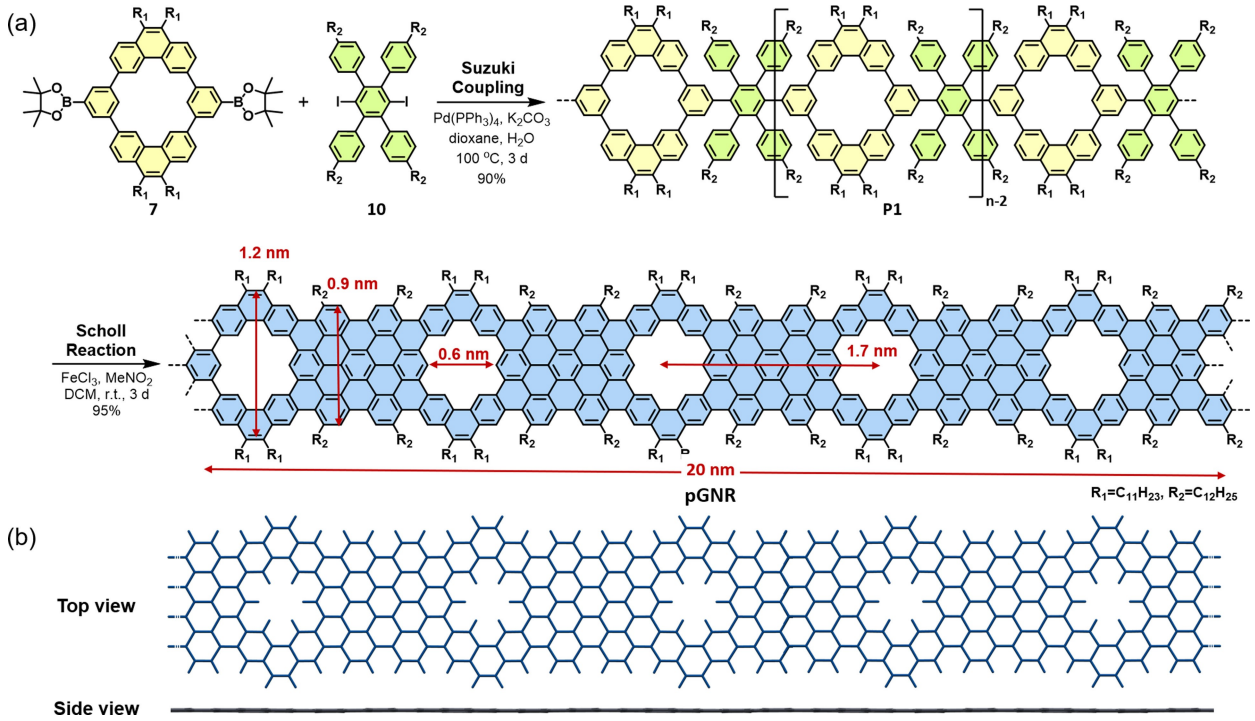

Scheme 2. (a) Synthetic route toward **pGNR**. (b) The top view and side view of the geometry of **pGNR** that is optimized by DFT simulation. Alkyl chains are omitted for clarity.

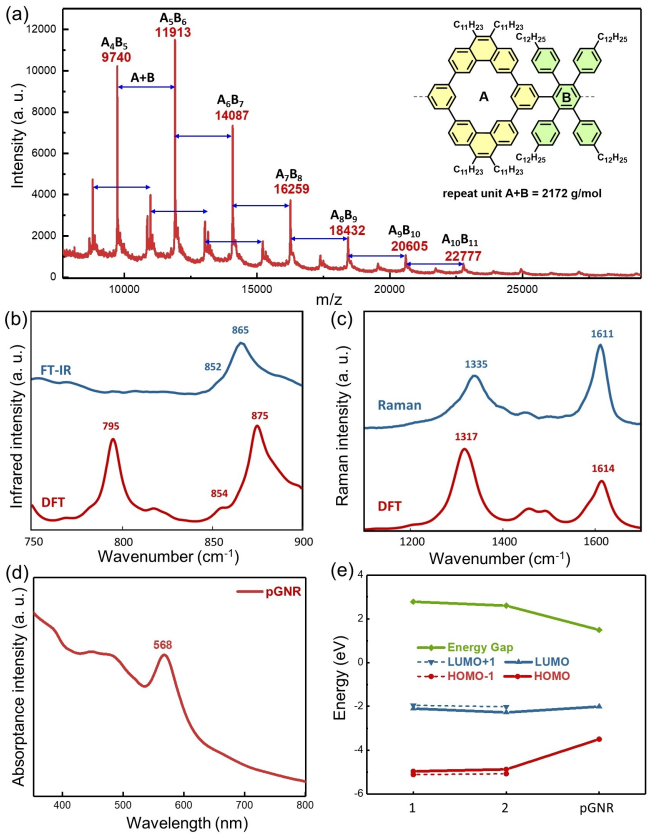

Figure 3. (a) MALDI-TOF mass spectrum of polymer precursor **P1** in the linear mode. Experimental and simulated FT-IR (b) and Raman (c) spectra of **pGNR** normalized to unity. The spurious IR peak at 795 cm^{-1} is an artifact of the DFT model, see Supporting Information. (d) UV/Vis absorption spectrum of **pGNR** in THF. (e) Calculated energy level of model compound **1**, dimer **2** and **pGNR**.

selected IR and Raman modes used for band assignments is shown in the Supporting Information (Figure S7–9, Table S3, S4). Further structural proof of **P1** and **pGNR** was confirmed by solid-state NMR measurements (Figures S10–12). The comparison of the ^{1}H NMR magic-angle spinning (MAS) spectra (Figure S9) of **P1** and **pGNR** demonstrated a clear increase in ^{1}H linewidth after graphitization. Moreover, the 2D ^{1}H–^{1}H double-quantum single-quantum (DQ-SQ) NMR correlation spectra demonstrate that ^{1}H–^{1}H autocorrelation signal of the aliphatic protons and the cross-correlation signal between the aromatic and aliphatic protons are observable as expected. In addition, the ^{1}H–^{1}H auto-correlation signal of the aromatic (7.7/14.4 ppm) protons stretches only up to 11.0/21.0 ppm (Figure S12). The low span of ^{1}H chemical shifts can be explained by the porous structure and thus a reduced distribution of chemical shift values as the ring current effects are reduced due to the porous backbone.

Benefiting from the nanopores in the backbone and long alkyl chains at the ribbon peripheries, the obtained **pGNR** can be readily dispersed in common organic solvents including THF and toluene, etc. Compared to model compounds **1a** and **1b**, the UV/Vis spectrum of **pGNR** in THF solution with a concentration of 0.1 mg mL^{-1} displayed a significantly red-shifted absorption with a maximum absorption peak at ~568 nm (Figure 3d). The optical band gap of **pGNR** is estimated to be 2.0 eV from the onset of the absorption of 620 nm, larger than the reported solution-synthesized nonporous GNRs with comparable widths that present the band gaps range from 1.1 to 1.88 eV.[7,8] In addition, DFT calculations suggest that the energy gaps of model compound **1**, dimer **2**, and **pGNR** (Figure S14) gradually decrease from 2.87, 2.60 to 1.49 eV, due to the extension of the π-conjugated backbone (Figure 3e).

To understand the electronic effect of nanopores in the GNR backbone, the band structure and frontier orbitals of the **pGNR** as well as corresponding nonporous GNR (**npGNR**) are calculated by the Perdew–Burke–Ernzerhof (PBE) exchange-correlation functional within the generalized gradient approximation (GGA) (Figure 4a,b). Compared to the calculated narrow band gap (0.97 eV) of **npGNR**, the **pGNR** possesses a lower valence band (VB)

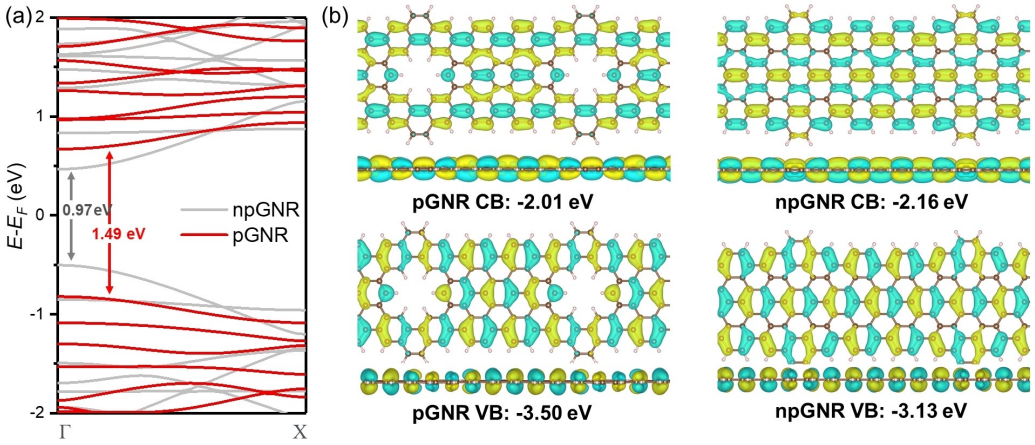

Figure 4. (a) Calculated band structures of **pGNR** (red) and the nonporous analogue **npGNR** (gray). (b) Top and side views of the calculated VB (−3.50 eV) and CB (−2.01 eV) orbitals of the **pGNR** as well as the calculated VB (−3.13 eV) and CB (−2.16 eV) orbitals of the **npGNR**, with the yellow and cyan colors indicating different signs of wave function.

(−3.50 *vs* −3.13 eV) and a higher conduction band (CB) (−2.01 *vs* −2.16 eV), resulting in an enlarged band gap of 1.49 eV due to the embedded inner nanopores, in good agreement of the experimental tendency. Figure 4b displays top and side views of the calculated orbitals of VB and CB of the **pGNR** and **npGNR**. Strikingly, for both ribbons, the frontier orbitals are delocalized over the entire conjugated backbone without interruption, proving the integrity of conjugation of this porous nanoribbon, superior to the on-surface-synthesized porous GNRs containing C–C single bonds in the backbone.[3–4] Similar orbitals distributions are also found in comparison of porous and nonporous model compounds and dimer (Table S6).

Conclusion

In summary, we have demonstrated the first successful bottom-up solution-synthesis of fully conjugated **pGNR** containing well-defined nanopores. The key to this design is the tailor-made polyphenylene precursor bearing pre-installed hexagonal nanopores, which allows us to access the **pGNR** with intact conjugation and precisely embedded nanopores with a diameter of 0.6 nm and an adjacent-pore-distance of 1.7 nm. The synthesis of **pGNR** has been thoroughly examined by various spectroscopic studies and simulations, along with the successful synthesis of two model compounds. DFT simulations have confirmed that the nanopores in **pGNR** can modulate the electronic structure and fine-tune the band gap without interrupting the conjugation of the ribbon. Thanks to the customized pore size/density, such solution-synthesized **pGNRs** with modulated band gap, enhanced liquid-phase processability and scalable production, hold great potential in many applications, such as thermoelectronics, ion detection, etc.

Acknowledgements

This research was financially supported by the National Natural Science Foundation of China (22225501 and 52203268), the EU Graphene Flagship (Graphene Core 3, 881603), H2020-MSCA-ITN (ULTIMATE, No. 813036), the Center for Advancing Electronics Dresden (cfaed), H2020-EU.1.2.2.—FET Proactive Grant (LIGHT-CAP, 101017821), the DFG-SNSF Joint Switzerland-German Research Project (EnhanTopo, No. 429265950), the Strategic Priority Research Program of the Chinese Academy of Sciences (Grant Nos. XDB33000000 and XDB33030300), and the DFG funded Cluster of Excellence "Matters of Activity" (No. 390648296). The authors gratefully acknowledge the GWK support for funding this project by providing computing time through the Center for Information Services and HPC (ZIH) at TU Dresden. Authors acknowledge Dortmund Electron Accelerator (DELTA) for grazing-incidence wide-angle x-ray scattering (GIWAXS) measurements. Z. Ling acknowledges the China Scholarship Council NO. 202006890007. W. Pisula acknowledges the National Science Centre, Poland through the grant UMO-2019/33/B/ST3/1550. The authors also thank Dr. Tomasz Marszalek and Yichen Jin for his experimental support and fruitful discussions. We are grateful for the assistance of Mr. Enrique Caldera for the GPC measurements, F. Drescher and Prof. E. Brunner for HR-MS measurements, and Dr. Hartmut Komber for high-temperature NMR measurements. Open Access funding enabled and organized by Projekt DEAL.

Conflict of Interest

The authors declare no conflict of interest.

Data Availability Statement

The data that support the findings of this study are available from the corresponding author upon reasonable request.

Keywords: Bandgap Engineering · Graphene Nanoribbons · Porous · Precision Synthesis · In Solution

[1] a) J. Bai, X. Zhong, S. Jiang, Y. Huang, X. Duan, *Nat. Nanotechnol.* **2010**, *5*, 190–194; b) C. Cheng, S. A. Iyengar, R. Karnik, *Nat. Nanotechnol.* **2021**, *16*, 989–995; c) C. Moreno, M. Vilas-Varela, B. Kretz, A. Garcia-Lekue, M. V. Costache, M. Paradinas, M. Panighel, G. Ceballos, S. O. Valenzuela, D. Peña, A. Mugarza, *Science* **2018**, *360*, 199; d) S. P. Koenig, L. Wang, J. Pellegrino, J. S. Bunch, *Nat. Nanotechnol.* **2012**, *7*, 728–732; e) H. Hou, X.-J. Zhao, C. Tang, Y.-Y. Ju, Z.-Y. Deng, X.-R. Wang, L.-B. Feng, D.-H. Lin, X. Hou, A. Narita, K. Müllen, Y.-Z. Tan, *Nat. Commun.* **2020**, *11*, 3976; f) W. Yuan, J. Chen, G. Shi, *Mater. Today* **2014**, *17*, 77–85; g) P. H. Jacobse, R. D. McCurdy, J. Jiang, D. J. Rizzo, G. Veber, P. Butler, R. Zuzak, S. G. Louie, F. R. Fischer, M. F. Crommie, *J. Am. Chem. Soc.* **2020**, *142*, 13507–13514; h) M. Shekhirev, P. Zahl, A. Sinitskii, *ACS Nano* **2018**, *12*, 8662–8669.

[2] a) W. F. da Cunha, M. L. Pereira Júnior, W. F. Giozza, R. T. de Sousa Junior, L. A. Ribeiro Júnior, G. M. e Silva, *Comput. Mater. Sci.* **2021**, *194*, 110423; b) D. Singh, V. Shukla, R. Ahuja, *Phys. Rev. B* **2020**, *102*, 075444; c) S. Hu, Z. Zhang, P. Jiang, J. Chen, S. Volz, M. Nomura, B. Li, *J. Phys. Chem. Lett.* **2018**, *9*, 3959–3968; d) J. Shao, V. Pohl, L. E. Marsoner Steinkasserer, B. Paulus, J. C. Tremblay, *J. Phys. Chem. C* **2020**, *124*, 23479–23489; e) M. Di Giovannantonio, K. Eimre, A. V. Yakutovich, Q. Chen, S. Mishra, J. I. Urgel, C. A. Pignedoli, P. Ruffieux, K. Müllen, A. Narita, R. Fasel, *J. Am. Chem. Soc.* **2019**, *141*, 12346–12354; f) G. A. Nemnes, C. Visan, A. Manolescu, *J. Mater. Chem. C* **2017**, *5*, 4435–4441; g) M. Sharafat Hossain, F. Al-Dirini, F. M. Hossain, E. Skafidas, *Sci. Rep.* **2015**, *5*, 11297; h) H. Sadeghi, S. Sangtarash, C. J. Lambert, *Sci. Rep.* **2015**, *5*, 9514.

[3] R. Pawlak, X. Liu, S. Ninova, P. D'Astolfo, C. Drechsel, S. Sangtarash, R. Häner, S. Decurtins, H. Sadeghi, C. J. Lambert, U. Aschauer, S.-X. Liu, E. Meyer, *J. Am. Chem. Soc.* **2020**, *142*, 12568–12573.

[4] a) M. R. Ajayakumar, M. Di Giovannantonio, C. A. Pignedoli, L. Yang, P. Ruffieux, J. Ma, R. Fasel, X. Feng, *J. Polym. Sci.* **2022**, *60*, 1912–1917; b) R. Yin, J. Wang, Z.-L. Qiu, J. Meng, H. Xu, Z. Wang, Y. Liang, X.-J. Zhao, C. Ma, Y.-Z. Tan, Q. Li, B. Wang, *J. Am. Chem. Soc.* **2022**, *144*, 14798–14808.

[5] a) F. Xu, C. Yu, A. Tries, H. Zhang, M. Kläui, K. Basse, M. R. Hansen, N. Bilbao, M. Bonn, H. I. Wang, Y. Mai, *J. Am. Chem. Soc.* **2019**, *141*, 10972–10977; b) Y. Huang, Y. Mai, U. Beser, J. Teyssandier, G. Velpula, H. van Gorp, L. A. Straasø, M. R. Hansen, D. Rizzo, C. Casiraghi, R. Yang, G. Zhang, D. Wu, F. Zhang, D. Yan, S. De Feyter, K. Müllen, X. Feng, *J. Am. Chem. Soc.* **2016**, *138*, 10136–10139; c) Y. Huang, W.-T. Dou, F. Xu, H.-B. Ru, Q. Gong, D. Wu, D. Yan, H. Tian, X.-P. He, Y. Mai, X. Feng, *Angew. Chem. Int. Ed.* **2018**, *57*, 3366–3371; d) W. Niu, J. Liu, Y. Mai, K. Müllen, X. Feng, *Trends Chem.* **2019**, *1*, 549–558; e) W. Niu, S. Sopp, A. Lodi, A. Gee, F. Kong, T. Pei, P. Gehring, J. Nägele, C. S. Lau, J. Ma, J. Liu, A. Narita, J. Mol, M. Burghard, K. Müllen, Y. Mai, X. Feng, L. Bogani, *Nat. Mater.* **2023**, *22*, 180–185.

[6] a) U. Beser, M. Kastler, A. Maghsoumi, M. Wagner, C. Castiglioni, M. Tommasini, A. Narita, X. Feng, K. Müllen, *J. Am. Chem. Soc.* **2016**, *138*, 4322–4325; b) X.-J. Zhao, H. Hou, P.-P. Ding, Z.-Y. Deng, Y.-Y. Ju, S.-H. Liu, Y.-M. Liu, C. Tang, L.-B. Feng, Y.-Z. Tan, *Sci. Adv.* **2020**, *6*, eaay8541.

[7] A. Narita, X. Feng, Y. Hernandez, S. A. Jensen, M. Bonn, H. Yang, I. A. Verzhbitskiy, C. Casiraghi, M. R. Hansen, A. H. R. Koch, G. Fytas, O. Ivasenko, B. Li, K. S. Mali, T. Balandina, S. Mahesh, S. De Feyter, K. Müllen, *Nat. Chem.* **2014**, *6*, 126–132.

[8] a) Y. Huang, F. Xu, L. Ganzer, F. V. A. Camargo, T. Nagahara, J. Teyssandier, H. Van Gorp, K. Basse, L. A. Straasø, V. Nagyte, C. Casiraghi, M. R. Hansen, S. De Feyter, D. Yan, K. Müllen, X. Feng, G. Cerullo, Y. Mai, *J. Am. Chem. Soc.* **2018**, *140*, 10416–10420; b) G. Li, K.-Y. Yoon, X. Zhong, X. Zhu, G. Dong, *Chem. Eur. J.* **2016**, *22*, 9116–9120; c) W. Niu, J. Ma, P. Soltani, W. Zheng, F. Liu, A. A. Popov, J. J. Weigand, H. Komber, E. Poliani, C. Casiraghi, J. Droste, M. R. Hansen, S. Osella, D. Beljonne, M. Bonn, H. I. Wang, X. Feng, J. Liu, Y. Mai, *J. Am. Chem. Soc.* **2020**, *142*, 18293–18298.

[9] D. Lungerich, D. Reger, H. Hölzel, R. Riedel, M. M. J. C. Martin, F. Hampel, N. Jux, *Angew. Chem. Int. Ed.* **2016**, *55*, 5602–5605.

[10] X. Zhang, Y. Hu, C. R. Lien-Medrano, J. Li, J. Shi, X. Qin, Z. Liao, Y. Wang, Z. Wang, J. Li, J. Chen, G. Zhang, J. V. Barth, T. Frauenheim, W. Auwarter, A. Narita, K. Müllen, C.-A. Palma, *J. Am. Chem. Soc.* **2023**, *145*, 8757–8763.

[11] a) I. Pozo, Z. Majzik, N. Pavliček, M. Melle-Franco, E. Guitián, D. Peña, L. Gross, D. Pérez, *J. Am. Chem. Soc.* **2019**, *141*, 15488–15493; b) A. Haags, A. Reichmann, Q. Fan, L. Egger, H. Kirschner, T. Naumann, S. Werner, T. Vollgraff, J. Sundermeyer, L. Eschmann, X. Yang, D. Brandstetter, F. C. Bocquet, G. Koller, A. Gottwald, M. Richter, M. G. Ramsey, M. Rohlfing, P. Puschnig, J. M. Gottfried, S. Soubatch, F. S. Tautz, *ACS Nano* **2020**, *14*, 15766–15775; c) Q. Fan, D. Martin-Jimenez, S. Werner, D. Ebeling, T. Koehler, T. Vollgraff, J. Sundermeyer, W. Hieringer, A. Schirmeisen, J. M. Gottfried, *J. Am. Chem. Soc.* **2020**, *142*, 894–899; d) X. Zhu, Y. Liu, W. Pu, F.-Z. Liu, Z. Xue, Z. Sun, K. Yan, P. Yu, *ACS Nano* **2022**, *16*, 10600–10607.

[12] W. Pisula, Ž. Tomović, C. Simpson, M. Kastler, T. Pakula, K. Müllen, *Chem. Mater.* **2005**, *17*, 4296–4303.

[13] T. Lu, F. Chen, *J. Comput. Chem.* **2012**, *33*, 580–592.

[14] X. Yang, X. Dou, K. Müllen, *Chem. Asian J.* **2008**, *3*, 759–766.

Manuscript received: April 24, 2023
Accepted manuscript online: June 19, 2023
Version of record online: July 18, 2023